Optical phonons in self-assembled Ge quantum dot superlattices: Strain relaxation effects

J. L. Liu, [a] J. Wan, Z. M. Jiang, A. Khitun, and K. L. Wang
Device Research Laboratory, Department of Electrical Engineering, University of California at Los Angeles, Los Angeles, California 90095-1594

D. P. Yu
Electron Microscopy Laboratory, Peking University, Beijing 100871, People's Republic of China

(Received 23 May 2002; accepted 11 September 2002)

We present Raman scattering by optical phonons in self-assembled Ge quantum dot superlattices grown by solid-source molecular beam epitaxy. The Ge quantum dots are vertically correlated and have different average sizes and dot morphologies. The GeGe optical phonon frequency was mainly caused by strain relaxation effects. Experimentally observed GeGe optical phonon modes were compared with calculated values using the deformation potential theory, indicating that the strain relaxation of Ge quantum dot superlattices arises not only from atomic intermixing but also from the morphology transition in dot formation. © *2002 American Institute of Physics.*
[DOI: 10.1063/1.1518756]

I. INTRODUCTION

Self-assembled quantum dots by the Stranski–Krastanov growth mode attracted much attention in the recent years. The study of phonon transport in such low-dimensional structures is of important fundamental interest in physics and potential applications in optoelectronics. To date, several groups have reported Raman scattering studies of quantum dots of other systems, such as, (Al, Ga)As/InAs,[1] (In, Ga, Al)Sb/GaAs,[2] InSb/InP,[3] and InAs/InP.[4] In the Si-based SiGe dot system, a great deal of effort has been invested in studying the optical phonon transport processes in single-layered Ge dots.[5–7] In contrast, multilayered Ge quantum dots are more desirable for optoelectronic applications. Though there have been several research reports on optical phonons of multilayered structures,[8–11] systematic studies, such as the phonon frequency dependence on dot size, the degree of atomic intermixing as well as dot morphology, have not yet been performed. The purpose of this article is to deal with these aspects of Raman scattering by optical phonons in Ge quantum dot superlattices. The experimentally observed optical phonon modes are compared with quantitative calculations, indicating that the strain relaxation of Ge quantum dot superlattices arises not only from atomic intermixing, but also during dot formation.

II. EXPERIMENTAL RESULTS AND DISCUSSION

Six samples were grown on Si (100) using a solid-source molecular beam epitaxy system. Samples A, B, and C were grown at 540 °C with ten periods of Ge and Si bilayers, and the Ge coverages of these samples were 12, 15, and 18 Å, respectively. Samples D and E were grown with the same Ge layer thickness of 15 Å but at different growth temperatures of 500 and 600 °C, respectively. In addition, sample E had a 22 period Ge quantum dot and Si bilayer while sample D contained ten periods. Sample F contained a 25 period Ge (6 Å) and Si bilayer, and was grown at 600 °C. The Si spacer layer thickness of 20 nm was used for all superlattices. No cap Si layer was used for these samples intentionally for atomic force microscopy (AFM) measurements in order to obtain the size, density, and morphology of the self-assembled dots.

Figure 1(a) shows a typical cross-sectional transmission electron microscopy (TEM) image of sample E. The 22 period vertically correlated Ge quantum dot layers are evident. The dots in the same layer and different layers beyond the sixth-seventh Ge layer along the growth direction are identical in size and shape. Figure 1(b) shows an AFM image of sample E. All dots appear as domes and the density is $2.6 \times 10^8\,\mathrm{cm}^{-2}$. The average dot base and height were determined to be 10 and 175 nm, respectively. Here, the AFM tip effect on the size determinations has been calibrated by TEM and excluded. Similar measurements have been performed on other samples as well. Figure 2 shows AFM images of the other four dot samples. For samples grown at the same growth temperature of 540 °C (images a, b, and c), the dome-over-pyramid ratio increases as the Ge coverage increases (from a to c). For samples with the same Ge coverage but grown at different temperatures of 540 °C (image b) and 500 °C (image d), the density is lower, while the height is larger at the lower temperature of 500 °C. The structural data are summarized in Table I.

Raman scattering measurements were performed on a Renishaw Raman Imaging 2000 system at room temperature. All spectra were excited with a 514 nm Ar^+ laser in the backscattering configuration and recorded with a Si charge-coupled devices camera. The spectral resolution is about $0.5\,\mathrm{cm}^{-1}$. Figure 3 shows typical Raman spectra of samples E, F, and an identical substrate used for these samples. The spectra were obtained using the same excitation power and

[a]Electronic mail: jliu@ee.ucla.edu

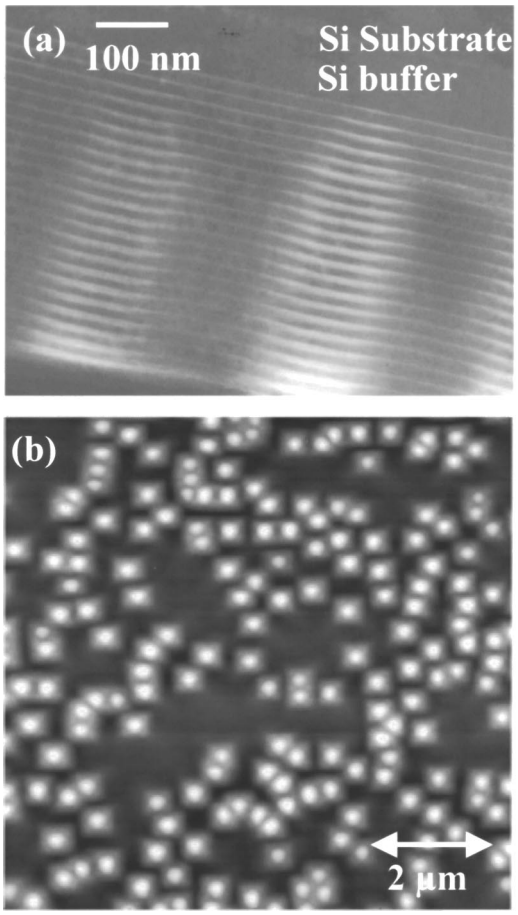

FIG. 1. (a) Cross-sectional TEM image and (b) AFM image of sample E. Vertically correlated quantum dots are evident. Highly uniform dome-shaped dots are observed and the density is determined to be $2.6 \times 10^8\ \mathrm{cm}^{-2}$.

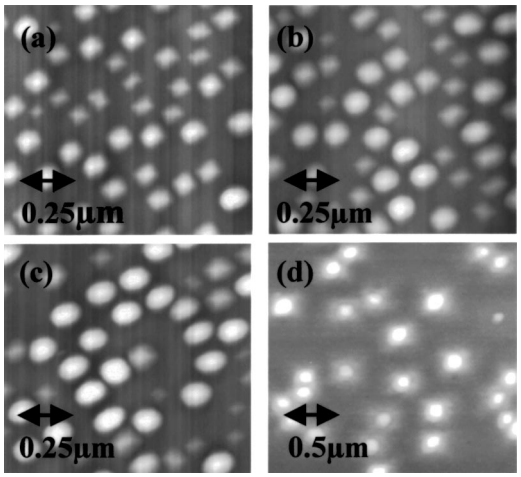

FIG. 2. AFM images of (a) sample A, (b) sample B, (c) sample C, and (d) sample D. Growth parameters and the size and density of the samples are summarized in Table I.

data accumulation time. As stated previously, sample E is a 22 period dot sample, while sample F is a sample only with Ge wetting layers, allowing us to compare and distinguish phonon features for the different samples. The GeGe optical mode can be clearly found at around $300\ \mathrm{cm}^{-1}$ for sample E. For sample F, the GeGe mode is much weaker. Because of the characteristics of the Stranski–Krastanov growth mode, sample E has similar Ge wetting layers, which can be clearly seen in the TEM image in Fig. 1. The difference of the GeGe modes for these samples suggests that the relatively strong GeGe mode from sample E is mainly from their Ge dots rather than their Ge wetting layers. In addition, it is important to note that the GeGe mode from sample E is much stronger than the second order transverse acoustic (2TA) phonon mode[12] for Si at $303\ \mathrm{cm}^{-1}$ as shown in the spectrum for the similar Si substrate. Other features observed for samples E and F are due to SiGe ($403\ \mathrm{cm}^{-1}$), local SiSi ($436\ \mathrm{cm}^{-1}$), and SiSi ($520\ \mathrm{cm}^{-1}$) atomic vibrations.

Figure 4 shows the Raman spectra of the dot samples in the spectral region of SiGe and GeGe optical phonons. Similar SiGe and GeGe lines are observed for these samples. The vertical dotted line is fixed at $300\ \mathrm{cm}^{-1}$, which represents the optical phonon position for bulk crystalline Ge. The frequency positions of the GeGe optical phonons in dot samples are shifted slightly to higher frequencies with respect to their bulk value ($300\ \mathrm{cm}^{-1}$). There are several possible physical origins, which can cause a Raman shift of optical phonons. The first one is phonon confinement. With a simple linear chain model, it is known that the optical phonon branches of bulk Ge are quadratic and moreover, nearly flat at the Brillouin zone center ($k \cong 0$). Confined phonons in a nanocrystal are equivalent to those vibrations in an infinite crystal whose wave vector is given by $m\pi/d$, where m is an integer and d is the diameter of the nanocrystal, in our case, the height of the dots. Therefore, the spatial limitations of superlattices cause a shift of optical phonons towards lower frequency. In the dots with a very small height of 1.5–2 nm,[9] the phonon confinement effect was observed to result in a shift less than $2\ \mathrm{cm}^{-1}$. For the present samples, however, the phonon confinement effect is not significant due to rather large dot sizes.

The second reason is the strain. The lattice mismatch of Si and Ge leads to a compressive strain on the dots in the

TABLE I. Growth parameters and structural data of the samples used for phonon characterization.

Sample	Ge layer thickness (Å)	Si layer thickness (nm)	Growth T (°C)	Dot base (nm)	Dot height (nm)	Density (cm^{-2})	Pyramid/dome ratio
A	12	20	540	110.4	11.9	3.6×10^9	1.15
B	15	20	540	122.0	14.0	4.1×10^9	0.56
C	18	20	540	122.2	16.0	3.5×10^9	0.38
D	15	20	500	114.7	15.1	5.9×10^8	0.25
E	15	20	600	175.5	10.2	2.6×10^8	0
F	6	20	600	----	----	----	----

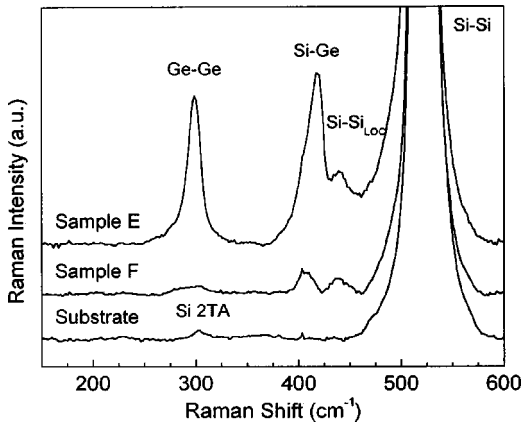

FIG. 3. Raman spectra of the samples E, F, and an identical Si substrate. The comparison of the data shows that GeGe optical phonon signal of sample E comes from dots rather than from Ge wetting layers or 2TA phonons from Si.

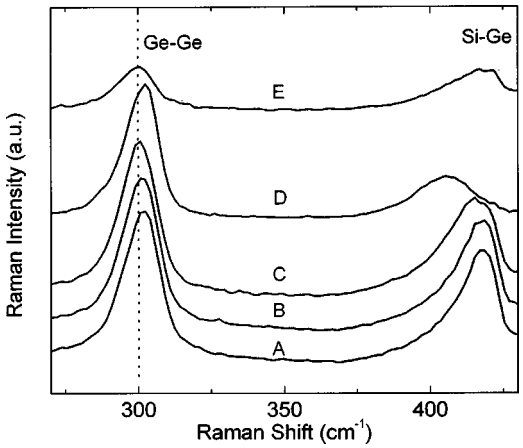

FIG. 4. Raman spectra of the dot samples. Similar SiGe and GeGe lines are observed for these samples. The frequency positions of the GeGe optical phonons in dot samples are shifted slightly to higher frequencies with respect to their bulk value ($300\,\mathrm{cm}^{-1}$).

lateral directions, which induces a GeGe mode shift to the higher frequency side. The GeGe optical phonon frequency ω induced by a biaxial strain in Ge can be written as[13]

$$\omega = \omega_0 + \frac{1}{2\omega_0}[p\varepsilon_{zz} + q(\varepsilon_{xx} + \varepsilon_{yy})], \tag{1}$$

where ω_0 is the frequency of the Ge zone center LO phonon; p and q are the Ge deformation potentials; ε_{xx}, and ε_{yy} is the biaxial strain $(a-a_0)/a$ with a and a_0 being the unstrained and strained lattice constants, respectively. In the earlier equation, $\varepsilon_{zz} = -(2C_{12})/(C_{11})\varepsilon_{xx}$, and $\varepsilon_{xx} = \varepsilon_{yy}$, where C_{11}, and C_{12} are elastic coefficients. Here, $\omega_0 = 0.564 \times 10^{14}\,\mathrm{s}^{-1}$, $p = -4.7 \times 10^{27}\,\mathrm{s}^{-2}$, $q = -6.167 \times 10^{27}\,\mathrm{s}^{-2}$, $C_{11} = 1288\,\mathrm{kbar}$, $C_{12} = 482.5\,\mathrm{kbar}$,[14] and $\varepsilon_{xx} = -0.042$ for fully strained pure Ge on Si, we obtain $\omega = 317.4\,\mathrm{cm}^{-1}$. The large difference between this calculated number and the experimental GeGe mode values (close to $300\,\mathrm{cm}^{-1}$ in Fig. 4) suggests that the dots are not fully strained as assumed in the calculation. By using Eq. (1) and the experimental GeGe optical phonon frequencies ω, the residual biaxial strain (ε_{xx}) on the quantum dots can be estimated and listed in Table II.

There are several mechanisms, which lead to the strain relaxation of the dots. The first one is the possible presence of threading dislocations. In our samples, high-quality, dislocation-free dots were observed by TEM measurements. Furthermore, we performed selective etch-pit study of the samples (not shown here), and no threading dislocation related pits were observed. Thus, this possibility is omitted. The second reason of the strain relaxation is the atomic intermixing at the Si/Ge interface. The degree of the interface intermixing can be determined by the integrated peak intensity ratio $I_{\mathrm{GeGe}}/I_{\mathrm{SiGe}}$ since the intensity depends on the relative number of corresponding bonds. This concept was used for SiGe alloy[15] and Ge quantum dots,[5] and can be expressed as

$$\frac{I_{\mathrm{GeGe}}}{I_{\mathrm{SiGe}}} \cong B\frac{x}{2(1-x)}, \tag{2}$$

where x is the average Ge concentration and coefficient B is related to the Bose factor and the frequencies of GeGe and SiGe optical modes of the alloy. It is found that coefficient B varies weakly with alloy composition and is determined to be 3.2.[16] $I_{\mathrm{GeGe}}/I_{\mathrm{SiGe}}$ can be obtained from the spectra in Fig. 4. The Ge concentrations in quantum dots estimated by this method are listed in Table II. It should be pointed out that a few techniques for the determination of composition of self-assembled quantum dots have been reported. These include scanning tunneling microscopy,[17] TEM with high-resolution imaging,[18] electron energy loss spectrometry,[19] x-ray energy disperse spectrometry,[20] high-resolution x-ray diffraction,[21,22] and scanning TEM.[23] Most of these techniques have shown nonuniform dot material distribution in the dots because of interdiffusion with the surrounding media. Raman scattering method used here is simple and direct, however, it can only give an average concentration of the dots. The results obtained were in good agreement with the average concentration values measured by x-ray diffraction

TABLE II. The experimental GeGe mode frequencies, integrated peak intensity ratios, and calculated Ge composition in dots and residual in-plane strain in the dot samples.

Sample	ω(GeGe) (cm^{-1})	$I_{\mathrm{GeGe}}/I_{\mathrm{SiGe}}$	Ge composition in dots	ε_{xx} (10^{-3})
A	302	1.45	0.48	−4.8
B	301.1	1.45	0.48	−2.65
C	300.5	1.45	0.48	−1.2
D	302.4	2.14	0.58	−5.8
E	300.4	1.29	0.45	−0.96

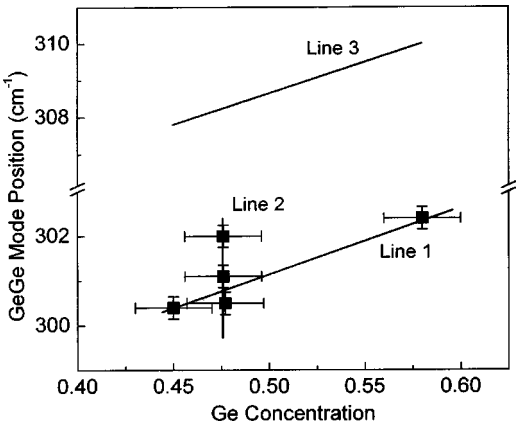

FIG. 5. GeGe mode position as a function of Ge concentration in dots. Ge concentration is obtained by means of the integrated intensity ratio of optical phonons of GeGe and SiGe. Solid lines 1 and 2 are used to guide the eyes. The results show that the different GeGe mode frequency is obtained for dots not only with different Ge concentrations, but also with a similar Ge concentration. Line 3 is the calculated data by assuming Si/Ge interdiffusion only.

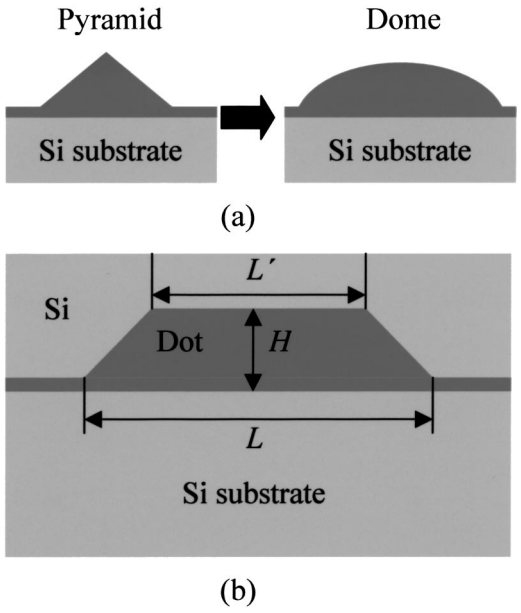

FIG. 6. (a) Schematic of the dot transition from pyramid to dome. The more domes on the surface, the more relaxation is achieved and (b) schematic of the dot capping process. The embedded dots in the Ge dot superlattices induce additional strain relaxation because of the Si capping.

measurements.[22] (The comparison is not shown here.) This allows us to believe that the concept of Eq. (2) is applicable to the quantum dot structures.

Figure 5 plots the GeGe peak position as a function of the Ge concentration in dots. Solid straight lines 1 and 2 are used to guide the eyes and indicate that the different GeGe mode frequency is obtained for dots not only with different Ge concentrations, but also with a similar Ge concentration. In order to clarify the observed dependences, we noticed that the lattice parameter of an alloy with a Ge concentration of x can be determined by Vegard's law

$$a_{\mathrm{Si}_{1-x}\mathrm{Ge}_x} = x a_{\mathrm{Ge}} + (1-x) a_{\mathrm{Si}}, \tag{3}$$

where a_{Ge} and a_{Si} are lattice parameters of pure Ge and Si. By considering this alloying effect only, the in-plane strain ε_{xx} can be written as $(a_{\mathrm{Si}_{1-x}\mathrm{Ge}_x} - a_0)/(a_{\mathrm{Si}_{1-x}\mathrm{Ge}_x})$. Moreover, we assume the same ω_0 and other deformation potentials for pure Ge. This approximation is reasonable because the interdiffusion occurs in the interface and the ''core'' of the dots remains pure Ge. For example, the nonuniform Ge content in the dots has been proved by elemental distribution analysis using an electron energy filtering imaging method in TEM[24] and scanning TEM.[23] Simple calculations show, for example, in-plane strain to be -0.02 for an alloy with Ge concentration of 0.48 (samples A, B, and C), leading to a GeGe mode frequency of 308.3 cm^{-1} by using Eq. (1). Calculated GeGe mode frequency as a function of Ge concentration is plotted in Fig. 5 as line 3. The calculated values show considerable shift from the value obtained for fully strained Ge on Si (317.4 cm^{-1}), however, are still larger than the peak frequencies of the GeGe modes of the samples A–E. As a matter of fact, the absolute value of residual strain on the dots shown in Table II is much smaller than the absolute value estimated here by interdiffusion only. Moreover, the picture of interdiffusion does not completely account for the peak position difference for the different samples with the same degree of interdiffusion. The earlier analysis suggests that additional strain relaxation mechanisms exist apart from Ge/Si interdiffusion. We believe that this additional strain relaxation comes from the process of the formation of Ge dots.

The relaxation of the formation of dots can be divided into two parts, i.e., the relaxation of the surface-layered dots and the relaxation of the buried dots. It is not difficult to understand the relaxation of the surface-layered dots if we go through the dot formation process. When Ge is deposited on Si, it first takes a layer-by-layer growth format. As the Ge film exceeds its critical thickness, it becomes rough by forming pyramidal islands to relieve strain energy. As more Ge is deposited, the islands transform from the pyramid shape to the dome shape, suggesting that there is more strain relaxation. It is indeed seen from Fig. 2 that the pyramid-over-dome ratio increases with the increase of the nominal Ge thickness for the samples grown at the same temperature of 540 °C. The pyramid-over-dome ratios are listed in Table I. This strain relaxation mechanism is schematically shown in Fig. 6(a). It should be noted that the relaxation is accomplished by the deformation of the film to form quantum dots only when the film thickness is less than about 20 Å. [25] When the film thickness exceeds this value, misfit/threading dislocations have to be present to relieve the increased strain energy from the increased film thickness as typically observed in conventional heteroepitaxy.

The relaxation is also induced by the dot embedding effect. Sutter and Lagally have used a strain-driven atom diffusion model to show that the dot shape transforms to truncated shape after the growth of the Si layer on top.[26] Indeed, we have observed this transition from the cross-section TEM measurements. A schematic showing this process is illustrated in Fig. 6(b). Similar to Fig. 6(a), a two-dimensional illustration is used for simplicity. Because of the

capping process, the in-plane strain distribution is modified and the change is[17]

$$\Delta\varepsilon_{xx}=\frac{2C_{11}}{C_{12}}\cdot\frac{H}{L-L'}\ln\left[\left(1+\frac{L-L'}{L'}\right)^2-1\right]. \quad (4)$$

Here, L, L', and H are the dimensions of the dots and illustrated in Fig. 6(b).

After recognizing all the earlier relaxation mechanism, we can fully explain the observed GeGe optical phonon frequencies. First, let us take a look at the line 1 of Fig. 5. This line represents the GeGe mode trend of a set of samples (C, D, and E) grown at different temperatures. GeGe mode frequency changes from 302.4 to 300.4 cm^{-1} when the Ge concentration decreases from 0.58 to 0.45 as a result of growth temperature from 500 to 600 °C, indicating that the sample grown at higher temperature induces stronger interface intermixing, or more strain relaxation. Quantitative calculations using Eqs. (1) and (3) show that a shift of 2.2 cm^{-1} is obtained for the present interdiffusion difference in the three samples (can be seen from line 3 in Fig. 5). This number is almost the same as the experimental observed shift, suggesting that the strain relaxation from the different degrees of interdiffusion is a main factor responsible for the different frequencies of the GeGe mode in this set of samples. In other words, the overall effect of the dot shape transition on the GeGe mode frequency is about the same for the three samples. Line 2 in Fig. 5 represents another set of samples (A, B, and C). As shown previously, this set of samples has the same degree of interdiffusion. Nevertheless, the GeGe optical phonon frequency is different and the largest difference is 1.5 cm^{-1}. Therefore, this difference arises from the different dot morphologies in the different samples, such as pyramid-over-dome ratios and dot height-over-base ratios.

III. SUMMARY

In summary, we have studied optical phonons and their relation to strain in Ge quantum dot superlattices. The GeGe optical phonon frequencies of the dot samples are larger than 300 cm^{-1} but within 3 cm^{-1}. Compared with the value of 317.4 cm^{-1} obtained by assuming fully strained Ge quantum dots, these frequencies indicate that the dots are partially relaxed. Strain relaxation was found not only from the atomic interdiffusion but also from the dot morphology transition both for the surface dots and the embedded dots. Furthermore, the change of the degree of atomic interdiffusion as a result of the growth temperature from 600 to 500 °C shows small GeGe mode frequency change of 2 cm^{-1}. For the same degree of atomic interdiffusion, a small GeGe mode shift of 1.5 cm^{-1} indicate the different dot morphologies among these samples. This study shows that Raman spectroscopy is an efficient tool for the determination of the average compositions and strains for zero-dimensional quantum dots.

ACKNOWLEDGMENTS

This work was funded by the DoD MURI-ONR program on Thermoelectrics (N00014-97-1-0516) and the AFOSR MURI program on phonon engineering (F49620-00-1-0328).

[1] D. A. Tenne, V. A. Haisler, A. I. Toropov, A. K. Bakarov, A. K. Gutakovsky, D. R. T. Zahn, and A. P. Shebanin, Phys. Rev. B **61**, 13785 (2000).
[2] B. R. Bennett, B. V. Shanabrook, and R. Magno, Appl. Phys. Lett. **68**, 958 (1996).
[3] G. Armelles, T. Utzmeier, P. A. Postigo, F. Briones, J. C. Ferrer, P. Peiro, and A. Cornet, J. Appl. Phys. **81**, 6339 (1997).
[4] J. Groenen, C. Priester, and R. Carles, Phys. Rev. B **60**, 16013 (1999).
[5] J. Groenen, R. Carles, S. Christiansen, M. Albrecht, W. Dorsch, and H. P. Strunk, Appl. Phys. Lett. **71**, 3856 (1997).
[6] C. E. Bottani, C. Mantini, P. Milani, M. Manfredini, A. Stella, P. Tognini, P. Cheyssac, and R. Kofman, Appl. Phys. Lett. **69**, 2409 (1996).
[7] P. D. Persans, P. W. Deelman, K. L. Stokes, L. J. Schowalter, A. Byrne, and T. Thundat, Appl. Phys. Lett. **70**, 472 (1997).
[8] J. L. Liu, Y. S. Tang, K. L. Wang, T. Radetic, and R. Gronsky, Appl. Phys. Lett. **74**, 1863 (1999).
[9] J. L. Liu, G. Jin, Y. S. Tang, Y. H. Luo, K. L. Wang, and D. P. Yu, Appl. Phys. Lett. **76**, 586 (2000).
[10] A. Milekhin, N. P. Stepina, A. I. Yakimov, A. I. Nikiforov, S. Schulze, and D. R. T. Zahn, Eur. Phys. J. B **16**, 355 (2000).
[11] L. Qin, K. L. Teo, Z. X. Shen, C. S. Peng, and J. M. Zhou, Phys. Rev. B **64**, 075312-1 (2001).
[12] K. Uchinokura, T. Sekine, and E. Matsuura, J. Phys. Chem. Solids **35**, 171 (1974).
[13] K. Uchinokura, T. Sekine, and F. Cerdeira, C. J. Buchenauer, F. H. Pollak, and M. Cardona, Phys. Rev. B **5**, 580 (1972).
[14] S. H. Kwok, P. Y. Yu, C. H. Tung, Y. H. Zhang, M. F. Li, C. S. Peng, and J. M. Zhou, Phys. Rev. B **59**, 4980 (1999).
[15] Proceedings of the 2nd International Conference on Light Scattering in Solids, Flammarion, Paris, 1971, p. 326.
[16] P. M. Mooney, F. H. Dacol, J. C. Tsang, and J. O. Chu, Appl. Phys. Lett. **62**, 2069 (1993).
[17] N. Liu, J. Tersoff, O. Baklenov, A. L. Holmes, Jr., and C. K. Shih, Phys. Rev. Lett. **84**, 334 (2000).
[18] A. Rosenauer, U. Fischer, D. Gerthsen, and A. Forster, Appl. Phys. Lett. **71**, 3868 (1997).
[19] T. Walther, C. J. Humphreys, and A. G. Cullis, Appl. Phys. Lett. **71**, 809 (1997).
[20] S. A. Chaparro, J. Drucker, Y. Zhang, D. Chandrasekhar, M. R. McCartney, and D. J. Smith, Phys. Rev. Lett. **83**, 1199 (1999).
[21] T. Wiebach, M. Schmidbauer, M. Hanke, H. Raidt, and R. Kohler, Phys. Rev. B **61**, 5571 (2000).
[22] Z. M. Jiang, X. M. Jiang, W. R. Jiang, Q. J. Jia, W. L. Zheng, and D. C. Qian, Appl. Phys. Lett. **76**, 3397 (2000).
[23] A. Harvey, H. Davock, A. Dunbar, U. Bangert, and P. J. Goodhew, J. Phys. D **34**, 636 (2001).
[24] X. Z. Liao, J. Zou, D. J. H. Cockayne, J. Qin, Z. M. Jiang, X. Wang, and R. Leon, Phys. Rev. B **60**, 15605 (1999).
[25] D. J. Eaglesham and M. Cerullo, Phys. Rev. Lett. **64**, 1943 (1990).
[26] P. Sutter and M. G. Lagally, Phys. Rev. Lett. **81**, 3471 (1998).